ACS NANO

Cite This: *ACS Nano* 2019, 13, 2927−2935

www.acsnano.org

ARTICLE

High Axial Ratio Nanochitins for Ultrastrong and Shape-Recoverable Hydrogels and Cryogels *via* Ice Templating

Liang Liu,[†,‡] Long Bai,[‡] Anurodh Tripathi,[‡] Juan Yu,[†] Zhiguo Wang,[†] Maryam Borghei,[‡] Yimin Fan,[*,†] and Orlando J. Rojas[*,‡,§]

[†]Jiangsu Co-Innovation Center of Efficient Processing and Utilization of Forest Resources, Jiangsu Key Lab of Biomass-Based Green Fuel & Chemicals, College of Chemical Engineering, Nanjing Forestry University, Nanjing 210037, China

[‡]Department of Bioproducts and Biosystems, School of Chemical Engineering, and [§]Department of Applied Physics, School of Science, Aalto University, P.O. Box 16300, FIN-00076 Aalto, Espoo, Finland

Supporting Information

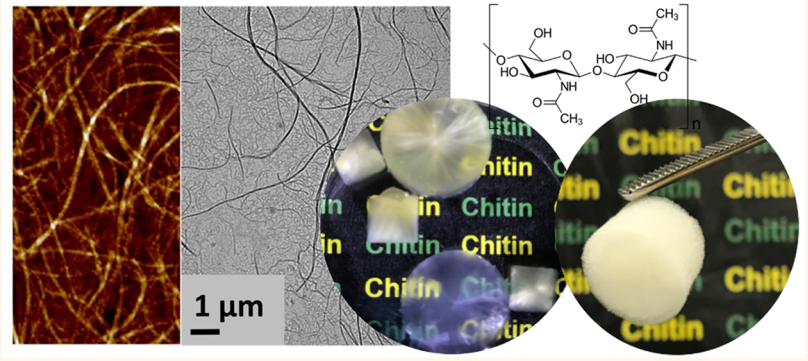

ABSTRACT: High yield (>85%) and low-energy deconstruction of never-dried residual marine biomass is proposed following partial deacetylation and microfluidization. This process results in chitin nanofibrils (nanochitin, NCh) of ultrahigh axial size (aspect ratios of up to 500), one of the largest for bioderived nanomaterials. The nanochitins are colloidally stable in water (ζ-potential = +95 mV) and produce highly entangled networks upon pH shift. Viscoelastic and strong hydrogels are formed by ice templating upon freezing and thawing with simultaneous cross-linking. Slow supercooling and ice nucleation at −20 °C make ice crystals grow slowly and exclude nanochitin and cross-linkers, becoming spatially confined at the interface. At a nanochitin concentration as low as 0.4 wt %, highly viscoelastic hydrogels are formed, with a storage modulus of ∼16 kPa, at least an order of magnitude larger compared to those measured for the strongest chitin-derived hydrogels reported so far. Moreover, the water absorption capacity of the hydrogels reaches a value of 466 g g^{-1}. Lyophilization is effective in producing cryogels with a density that can be tailored in a wide range of values, from 0.89 to 10.83 mg·cm^{-3}, and corresponding porosity, between 99.24 and 99.94%. Nitrogen adsorption results indicate reversible adsorption and desorption cycles of macroporous structures. A fast shape recovery is registered from compressive stress−strain hysteresis loops. After 80% compressive strain, the cryogels recovered fast and completely upon load release. The extreme values in these and other physical properties have not been achieved before for neither chitin nor nanocellulosic cryogels. They are explained to be the result of (a) the ultrahigh axial ratio of the fibrils and strong covalent interactions; (b) the avoidance of drying before and during processing, a subtle but critical aspect in nanomanufacturing with biobased materials; and (c) ice templating, which makes the hydrogels and cryogels suitable for advanced biobased materials.

KEYWORDS: *nanochitin, hydrogels, cryogels, shape recovery, chemical cross-linking, ice templating, ultrahigh axial size*

Chitin, poly(β-(1→4)-*N*-acetyl-D-glucosamine), is the most abundant amino polysaccharide in the biosphere.[1] Due to its biocompatibility, biodegradability, renewability, and antibacterial properties, it is considered in diverse applications, including personal care, cosmetics, and

Received: September 21, 2018
Accepted: January 28, 2019
Published: January 28, 2019

DOI: 10.1021/acsnano.8b07235
ACS Nano 2019, 13, 2927−2935

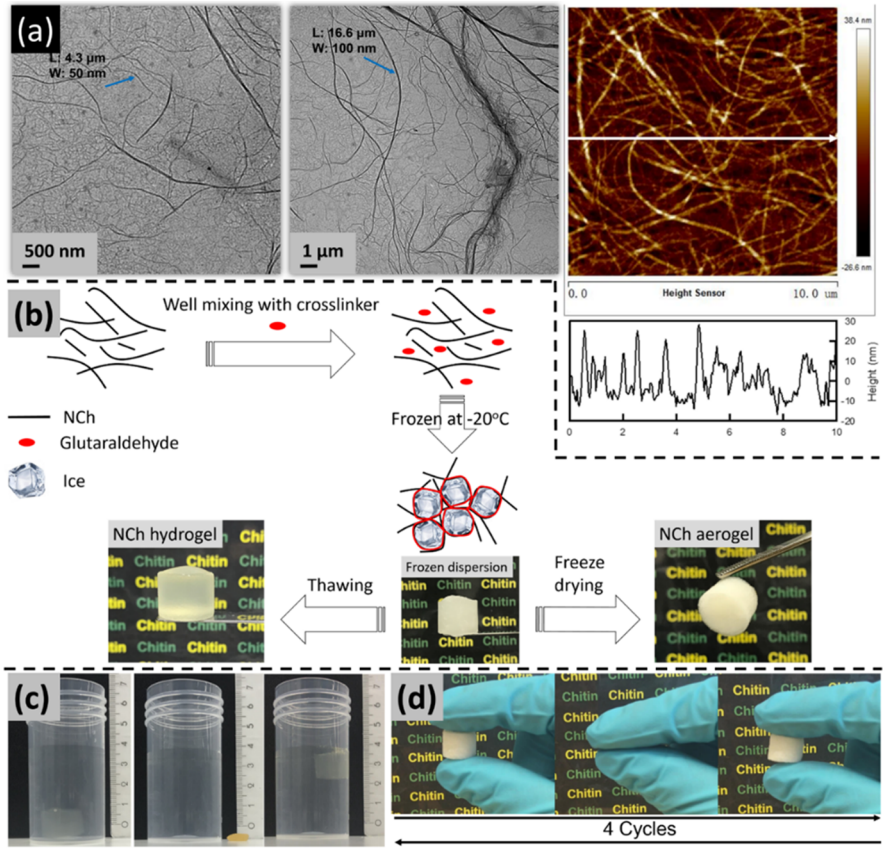

Figure 1. (a) Transmission electron microscopy (left) and atomic force microscopy (AFM) (right) images of nanochitins (NCh) at the given magnifications (see scale bars). Note the AFM image corresponds to 1 μm side dimension and includes a height profile. Some nanofibrils are highlighted, and their dimensions are provided. (b) Schematic illustration of the formation of nanochitin hydrogels and cryogels *via* ice templating and cross-linking (not to scale). Included are the photos of the respective system. An ultralight cryogel is achieved as noted by electrostatic suspension on the tip of a metal rod. (c) Photographs of a cylindrical nanochitin hydrogel (prepared from 0.2 wt % aqueous nanochitin suspension), which was immersed in water soon after preparation (left picture with the hydrogel immersed in water in a cylindrical container). Upon extraction and mechanical compression, the hydrogel forms a membrane (middle image, outside the container and by the ruler), which recovers its original shape rapidly, after reimmersion in water (right image). (d) Photographs of a nanochitin cryogel soon after preparation from a 0.1 wt % nanochitin suspension (left). The cryogel is fully collapsed (middle), and after release of the compression, its shape is rapidly and fully recovered (right). The process can be extended for many cycles (the images corresponds to the fourth cycle of compression and decompression).

biomaterials.[2,3] However, the narrow window of conditions suitable to isolate or dissolve chitin has restricted its otherwise incredible potential. Until now, only few solvents have been found effective in dissolving chitin. They include LiCl/dimethylacetamide (DMAc), ionic liquids, strong alkali solutions, and calcium chloride dehydrate-saturated methanol.[4−7] However, these dissolution treatments require special conditions and lead to the destruction of the crystal structure of chitin. Contrary to the typical, full deconstruction of chitin into macromolecular solutions, mechanical shearing into nanoparticle suspension allows the preservation of the hierarchical and multidimensional features of the material building blocks, notably, high axial ratio chitin nanofibrils (also termed here as nanochitin, NCh).[8] Methods such as acid hydrolysis, mechanical shearing, and ultrasonication have been employed for the production of nanocelluloses and nanochitins. They can be dispersed in aqueous media under acid, alkali, or neutral conditions, depending on the intended applications.[9] Nanochitins exhibit structural features similar to those of nanocelluloses,[8] including their morphology with fibrils' widths and lengths reaching several nanometers and microns, respectively.[8,10] Due to their crystalline structure, nanochitins exhibit excellent physical properties. For example, the strength of α- and β-nanochitins is estimated to be 1.6 and 3.0 GPa, respectively,[11] similar to that of nanocellulose with a tensile strength of at least 2 GPa.[12] However, the energy-intensive process conditions used so far limit an efficient production and prevent a wide adoption of nanochitin for material development.[8,13] Therefore, the design of facile routes to easily isolate and exploit nanochitin is a priority.

Previously, hydrogels and aerogels have been prepared by using dissolved chitin or chitin nanowhiskers. For dissolved chitin, highly flexible and tough double-cross-linked hydrogels were obtained with epichlorohydrin and solvent exchange with aqueous ethanol after dissolution in KOH/urea solvent.[1] Aerogels with densities as low as 125 mg·cm^{-3} and porosity as high as 92% were reported by dissolving chitin in DMA/LiCl followed by supercritical point drying.[14] For nanochitins, only physically cross-linked hydrogels have been reported,[9,15,16] resulting in aerogels with a lower density compared to that obtained from dissolved chitin, as low as 43 mg·cm^{-3} (porosity up to 97%).[17] Chemically cross-linked hydrogels and aerogels have not been attempted but offer possibilities for exploitation of chitin as a renewable nanomaterial. This is introduced in

DOI: 10.1021/acsnano.8b07235
ACS Nano 2019, 13, 2927−2935

Table 1. Nomenclature and Main Properties of Chemically Cross-Linked Nanochitin Hydrogels and Cryogels

			hydrogel	cryogel		
system	NCh (wt %)	Glu/NCh mass ratio	storage modulus (Pa)	density ($mg \cdot cm^{-3}$)	porosity (%)	BET surface area, ($m^2 \cdot g^{-1}$)
NCh(0.05)/Glu(0.4)	0.05	0.4		0.89 ± 0.22	99.94	
NCh(0.1)/Glu(0.4)	0.1	0.4		1.28 ± 0.24	99.91	
NCh(0.2)/Glu(0.4)	0.2	0.4	1476	2.69 ± 0.16	99.81	25.3
NCh(0.4)/Glu(0.1)	0.4	0.1	1423	4.24 ± 0.16	99.70	21.8
NCh(0.4)/Glu(0.4)	0.4	0.4	10829	5.79 ± 0.51	99.59	16.6
NCh(0.4)/Glu(1.0)	0.4	1.0	15928	9.85 ± 0.46	99.31	
NCh(0.6)/Glu(0.4)	0.6	0.4	11357	10.83 ± 1.89	99.24	12.2

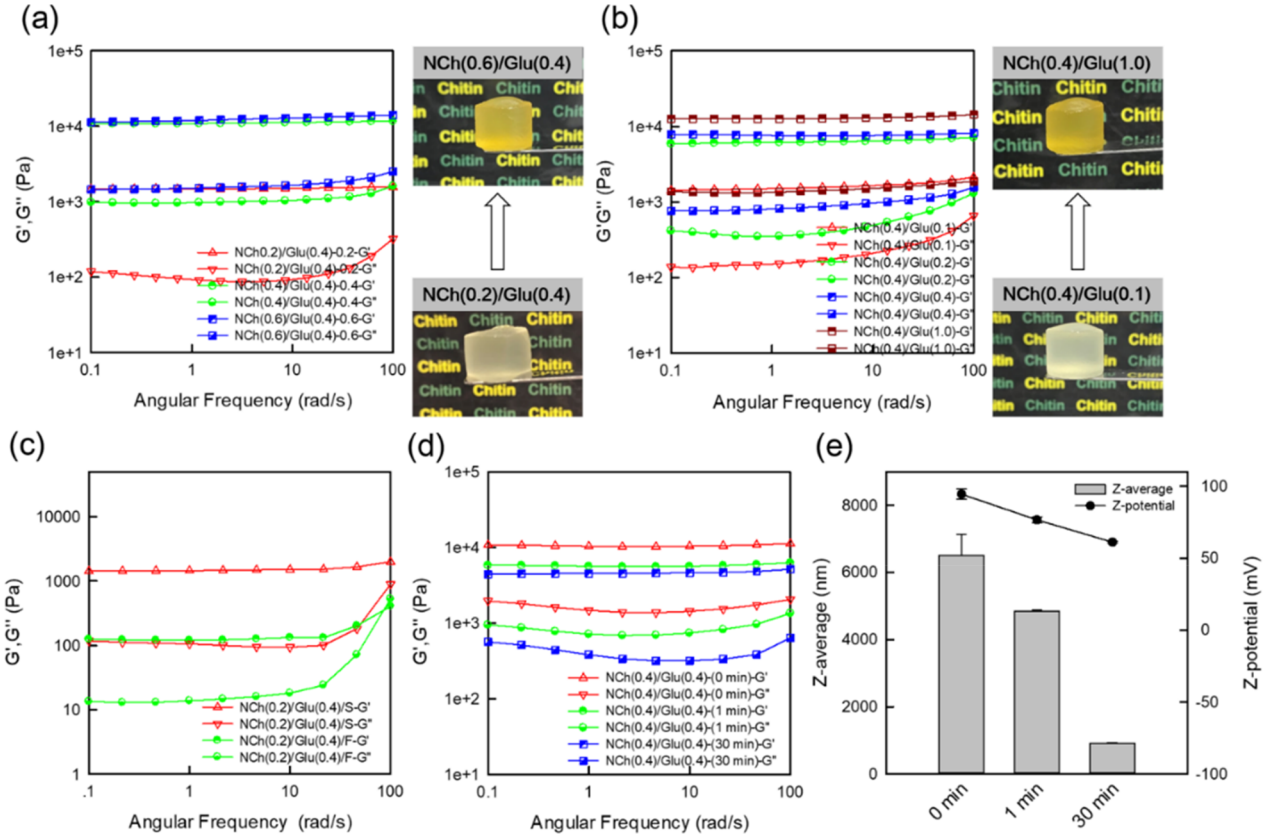

Figure 2. Frequency sweeps showing the storage (elastic) modulus (G', filled symbols) and the viscous (loss) modulus (G'', open symbols) for the respective system to test the effect of (a) nanochitin concentration (using 0.4 Glu/NCh mass ratio) and (b) glutaraldehyde dosage (using hydrogels obtained from 0.4 wt % nanochitin concentration). Rate of freezing: (c) slow S (−20 °C) and fast F (−196 °C) freezing of NCh(0.2)/Glu(0.4) hydrogels. Fibril length according to the sonication time in minutes (0, 1, and 30 min): (d) NCh fibril length in NCh(0.4)/Glu(0.4) hydrogels. (e) NCh fibril length (Z-average in nm, left axis) and ζ-potential (in mV, right axis) in aqueous suspension (indicative of colloidal stability) upon treatment with tip sonication for 0, 1, and 30 min.

this work, with special emphasis on the effects of water removal and ice templating.

RESULTS AND DISCUSSION

After purification and partial deacetylation (final degree of deacetylation of 26%),[9] chitin was suspended in acid solution (pH 3), and upon homogenization (15000 rpm, 5 min) followed by one-pass microfluidization and centrifugation, the length of the nanochitins reached values of ∼50 μm and widths as low as 50 nm (axial ratio >100, Figure 1a). The calculated nanofibrillation yield was >85%, indicating a facile deconstruction of the precursor biomass into nanochitin at low-energy microfluidization (only one pass was needed). The high electrostatic charge of the fibrils (ζ-potential of +95 ± 3.5 mV) endowed very stable colloidal suspensions in water.

Nanochitin Hydrogels. The pH shift was effective in triggering the formation of highly entangled networks from the individual chitin nanofibrils. Hydrogel synthesis was used here as the first step for processing. In previous work, gas-phase coagulation was applied to physically cross-link nanochitin hydrogels and cryogels, resulting in the stiffest chitin materials reported up to that point.[9] However, such physical cross-linking set a limiting toughness and strength under stress or strain.[18] Here, we applied chemical cross-linking, which has not been attempted before. Considering the abundant amino groups in nanochitin, glutaraldehyde (Glu) was used for this purpose. Fourier transform infrared (FTIR) spectra of purified chitin, nanochitin, and chemically cross-linked nanochitin indicated a new peak in 1750 cm^{-1}, assigned to free aldehydic bonds. Together with an increased peak corresponding to C−

DOI: 10.1021/acsnano.8b07235
ACS Nano 2019, 13, 2927−2935

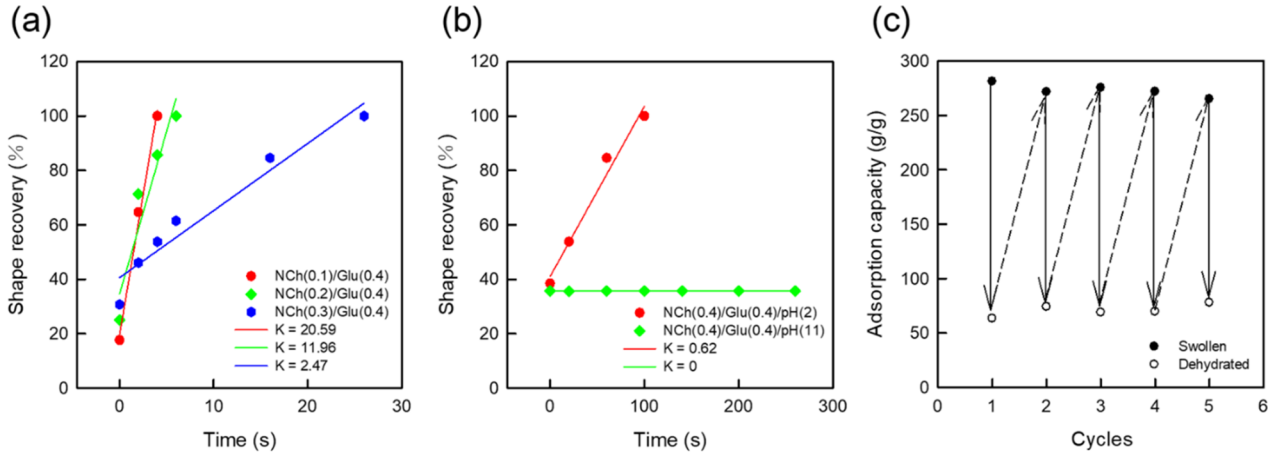

Figure 3. (a) Dynamics of shape recovery, as indicated by the % recovery from the original height of NCh hydrogels immersed in water during the given time and as a function of the composition (with 0.4 Glu/NCh mass ratio) (K is the slope of the given fit). (b) Dynamics of shape recovery for the NCh(0.4)/Glu(0.4) hydrogel after immersion in buffer solution at pH 2 and 11. (c) Cyclic water sorption capacity of the NCh(0.4)/Glu(0.4) hydrogel. In the experiments, water in the hydrogel was removed and it was then left to reabsorb water (dehydration−swelling cycles).

H stretching at 2930 and 1655 cm^{-1} for imine bonds, the results indicated successful chemical cross-linking between the chitin nanofibrils (Figure S1).

Strong hydrogels were possible at very low solids content (≤0.6 wt %) *via* freezing-induced chemical cross-linking, making them suitable as drug carriers, tissue scaffolds, or insulators, which are otherwise derived from complex processing routes.[19,20] However, it was realized that without freezing but in the presence of a cross-linker, the nanochitin suspension becomes stable for at least 1 week (time of observation) at room temperature (Figure S2a,b) (note that in the absence of cross-linker, the physically cross-linked cryogels returned back into a liquid suspension after freezing−thawing, Figure S2c). With time, the reaction between the cross-linker and nanochitin's amino groups turned the suspension into a yellowish color (Figure S2b).[21] Despite the cross-linking, the electrostatic repulsion between nanochitins in acidic condition prevented gelling,[22] an effect that was observed only after freezing and thawing the suspension, forming exceptionally strong hydrogels.

Cryogels were obtained from the chemically cross-linked nanochitin simply by lyophilization of the frozen system described above (Figure 1b). The resulting nanochitin hydrogels and cryogels were named according to NCh(x)/Glu(y), where x indicates the mass concentration of the initial nanochitin suspension, and y is the glutaraldehyde/nanochitin mass ratio (Table 1). All the nanochitin hydrogels and cryogels were both highly flexible and displayed shape recovery properties (Figure 1c,d). The hydrogels prepared from dilute nanochitin suspension (0.2 wt %) and compressed to the maximum limit returned to their original shape a few seconds after immersion in water. Likewise, cryogels prepared from 0.1 wt % nanochitin recovered reversibly after multiple compression cycles (Video S1 and Video S2).

Figure 2a,b includes photographs of nanochitin hydrogels. Weak hydrogels were formed from 0.1 wt % nanochitin suspensions (Figure S3). However, strong hydrogels were produced from suspensions at >0.2 wt % NCh concentration. With increased cross-linker addition, yellowing increased (compare NCh(0.4)/Glu(0.1) and NCh(0.4)/Glu(0.4)), owing to more extensive cross-linking.

The water absorption capacity of NCh(x)/Glu(0.4) hydrogels was reduced at increased nanochitin concentration (466, 296, and 208 g g^{-1} for 0.2, 0.4, and 0.6 wt %, respectively) (Figure S3). For a fixed nanochitin concentration (0.4 wt %), the water capacity of the NCh(0.4)/Glu(y) hydrogels decreased from 384 to 162 g g^{-1} as the glutaraldehyde ratio increased from 0.1 to 0.4 wt %. The observed trends in water absorption correlate inversely with the mechanical strength of the hydrogels, which is otherwise significantly enhanced with the increase of chitin or cross-linker concentrations.[23]

It was determined that $G' > G''$ for all hydrogels (Figure 2a−d). At an angular frequency of 0.1 rad·s^{-1}, the hydrogels became stiffer with nanochitin concentration. G' values for NCh(x)/Glu(0.4) hydrogels were 1476, 10829, and 11357 Pa prepared at nanochitin concentrations of 0.2, 0.4, and 0.6 wt %, respectively. These values are at least an order of magnitude larger compared to those measured for the strongest chitin-derived hydrogels reported so far. The combination of ultralong chitin nanofibrils and strong covalent interactions is the main reason for this result. In addition, a denser cross-linking produced stiffer hydrogels (Figure 2b). For NCh(0.4)/Glu(y) hydrogels, G' = 1423, 5884, 7792, 12601, and 15928 Pa at cross-linker dosage ratios of 0.1, 0.2, 0.4, and 1.0 wt %, respectively.

Slow and fast freezing (−20 °C, refrigerator, and −196 °C, liquid nitrogen) were conducted to further understand the freezing-induced chemical cross-linking. After being washed with water, the elastic modulus of the obtained hydrogels was 1426 (−20 °C) and 125 (−196 °C) Pa, respectively (Figure 2c). The weaker hydrogels formed from the fast freezing process, which is related to the insufficient cross-linking and the role of ice growth. The freezing point of glutaraldehyde is −14 °C, and at −20 °C, the system was frozen for 2 h while only 3 min elapsed for the fast freezing at −196 °C. The slow supercooling and ice nucleation at −20 °C made the ice crystals grow slowly and exclude nanochitin and glutaraldehyde, which became spatially confined at the interface. It is reasonable to expect that this effect promotes closer interparticle distances and more extensive cross-linking.[24] In contrast, at −196 °C, both water and glutaraldehyde froze rapidly, restricting more efficient chemical cross-linking. Upon

DOI: 10.1021/acsnano.8b07235
ACS Nano 2019, 13, 2927−2935

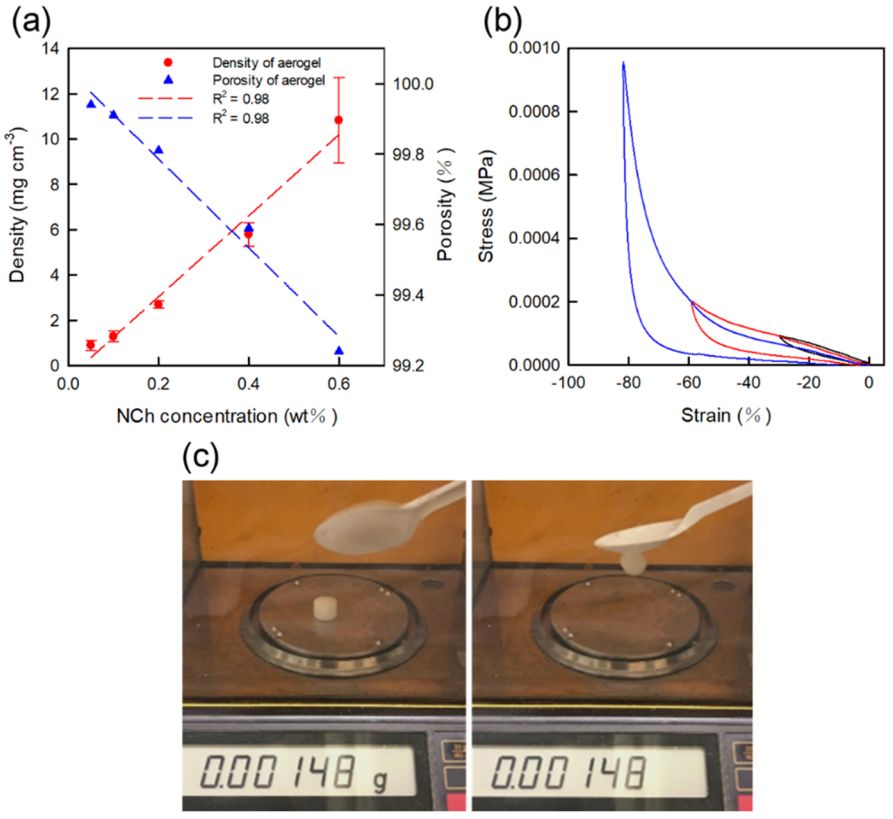

Figure 4. (a) Density and porosity of nanochitin cryogels as a function of nanochitin concentration in the precursor suspension with 0.4 Glu/NCh mass ratio. (b) Compressive stress−strain hysteresis of NCh(0.1)/Glu(0.4) cryogels. (c) Photographs of NCh(0.1)/Glu(0.4) cryogel (left) that was lifted with a plastic spoon by static electricity (right). The density and porosity of this cryogel was 1.53 mg·cm^{-3} and 99.89%, respectively.

thawing, the mechanical strength of these latter hydrogels was limited. In contrast, slow freezing significantly improved the efficiency of cross-linking and produced stronger nanochitin hydrogels. This effect is herein referred to as "freezing-induced cross-linking". An interesting observation is the templating of the material following radial ice channels (Figure S4), indicating the possibility of an ordered internal structure in the hydrogels.

Next, we discuss the effect of nanochitin fibril length on the properties of the hydrogels. A suspension with nanochitins with a fibril length of up to 6503 ± 636 nm and ζ-potential of +94.6 ± 3.5 mV was subjected to tip sonication to produce smaller nanochitins. Sonication for 1 and 30 min reduced the average length of the fibrils to 4850 ± 39 and 918 ± 22 nm, respectively (Figure 2e). The respective values of ζ-potential were +76.60 ± 2.2 and +61.1 ± 0.7 mV.[25] Hydrogels were prepared from NCh(0.4)/Glu(0.4) after concentrating the suspensions to the given concentrations. Compared to G′ of the hydrogels prepared from the original nanochitin (10869 Pa), smaller values were recorded for the shorter nanochitins: 5817 and 4423 Pa, respectively (Figure 2d). Scanning electron microscopy (SEM) images of hydrogels produced with NCh of different lengths are shown in Figure S5, which reveal that the pore walls formed under the predominant presence of long NCh fibrils. The stronger pore walls formed by the highly interconnected, longer nanochitins is a main reason for the higher strength of the corresponding hydrogels.[26]

On the basis of their mechanical integrity and strength, nanochitin hydrogels were further studied for their shape recovery when subjected to water removal and reabsorption. Dehydrated NCh hydrogels rapidly recovered their initial shape upon immersion in water during given times (Figure 3a). Upon compression, the height of the hydrogels prepared from 0.1, 0.2, and 0.3 wt % NCh concentration was reduced to 18, 25, and 31%, respectively. After reimmersion in water, complete shape recovery was reached in 4, 6, and 26 s (Figure S6a−c). The faster shape recovery observed for the hydrogels prepared at lower NCh concentration is explained by their higher porosity (Table 1) and the better organized and interconnected structure (see Figure 5 and respective discussion).

The shape recovery property was also found to depend on the pH (Figure 3b). NCh(0.4)/Glu(0.4) hydrogels were subjected to solvent exchange with buffer solution of pH 2 and 11 followed by compression to 38 and 35% of their initial height, respectively. After reimmersion in acid buffer solution (pH 2), the hydrogels reached full shape recovery in 100 s. In contrast, no shape recovery was observed in alkaline buffer solution (pH 11), even after immersion for several minutes (Figure S6d,e). The results are explained by the protonation of amino groups of NCh under the acidic condition and the higher hydrophilicity of the system.[9] To test NCh hydrogel reusability, they were subjected to five compression/immersion cycles (Figure 3c). A small reduction in water absorption capacity (4% reduction) was determined for freshly prepared NCh(0.4)/Glu(0.4) hydrogels, possibly due to the slight deformation of the walls within the structure.[24]

Nanochitin Cryogels. Lyophilization of frozen NCh hydrogels yielded cryogels with ultralow density and corresponding high porosity. With the increased NCh

DOI: 10.1021/acsnano.8b07235
ACS Nano 2019, 13, 2927−2935

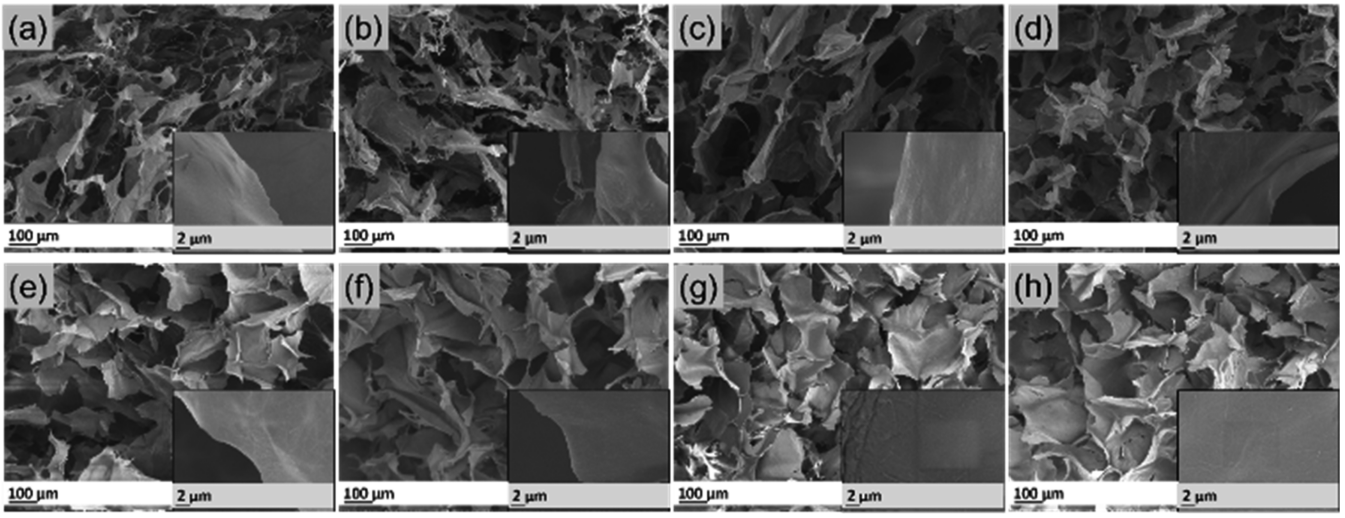

Figure 5. SEM images of nanochitin cryogel prepared from different hydrogel compositions: (a) NCh(0.05)/Glu(0.4), (b) NCh(0.1)/Glu(0), (c) NCh(0.1)/Glu(0.4), (d) NCh(0.2)/Glu(0.4), (e) NCh(0.4)/Glu(0.1), (f) NCh(0.4)/Glu(0.4), (g) NCh(0.4)/Glu(1.0), and (h) NCh(0.6)/Glu(0.4). The insets correspond to images at higher magnification, highlighting the pore walls.

concentration, an increased density was measured, from 0.89 ± 0.22 to 10.83 ± 1.89 mg·cm^{-3}. The corresponding porosity values ranged from 99.24 to 99.94% (Figure 4a). At a given NCh concentration, higher density and lower porosity were recorded with the increased cross-linking. The densities of NCh(0.05)/Glu(0.4) and NCh(0.1)/Glu(0.4) cryogels were 0.89 ± 0.22 and 1.28 ± 0.24 mg·cm^{-3}, considerably lower than the values reported so far for chitin cryogels (4.8 to 100 mg·cm^{-3}) and even lower than those reported for nanocellulose-based cryogels (1.7 to 10 mg·cm^{-3}).[2,14,17,20,27] It should be noted that the cryogel produced with the lowest nanochitin concentration, NCh(0.05)/Glu(0.4), was strong enough to sustain handling, but it did not withstand cycles of compression−decompression (Figure S7a−c). In contrast, the NCh(0.1)/Glu(0.4) cryogel displayed excellent shape recovery properties: even after severe compression, the cryogel recovered fully, with no apparent permanent deformation (Figure 1d). Moreover, the shape recovery occurred immediately after load release (Video S1). In the absence of cross-linker and upon compression, the cryogel prepared from 0.1 wt % nanochitin suspension was irreversibly collapsed into a membrane (Figure S7d−f).

The compressive stress−strain hysteresis was measured (Figure 4b) and indicated that the NCh(0.1)/Glu(0.4) cryogel exhibited the largest shape recovery, withstanding over 80% compressive strain and recovering completely once the load was released. For NCh(0.4)/Glu(0.1) and NCh(0.6)/Glu(0.4) cryogels, complete shape recovery was also achieved after 30% compression. In these latter cases, only partial shape recovery took place for relatively higher compression levels (60 or 80% strain compression) (Figure S8a,b).

The pore structures of NCh(0.2)/Glu(0.4), NCh(0.4)/Glu(0.1), NCh(0.4)/Glu(0.4), and NCh(0.6)/Glu(0.4) cryogels were analyzed *via* nitrogen adsorption/desorption isotherms (Brunauer−Emmett−Teller, BET, Figure S8c). The specific surface was reduced as nanochitin or cross-linker concentration increased, 25, 22, 17, and 12 m^2·g^{-1}, Table 1). The BET results indicate reversible adsorption and desorption cycles, with no sign of leveling-off at high relative pressures, which is typical of nonporous and macroporous structures, as supported by SEM imaging (Figure 5). All the cryogels exhibited highly porous structures, but the pores were distributed nonhomogeneously, with sizes ranging from a few to hundreds of micrometers. At a cross-linker ratio of 0.4, tight film-like pore walls and less fibrillar structures were observed. Also, smaller but better enclosed pores were observed at increasing nanochitin concentrations (Figure 5a,c,d,f,h).

As the NCh(0.05)/Glu(0.4) cryogel was too weak to support cyclic compression, whereas those prepared at higher NCh concentrations sustained full recovery, it is reasonable to assume that the film-like pore walls observed in SEM favored shape recovery. As shown in the insets of Figure 5, all film-like pore walls were supported by assembled nanochitin fibrils. However, both NCh(0.1)/Glu(0) and NCh(0.1)/Glu(0.4) showed NCh-supported film structures. Interestingly, the NCh(0.1)/Glu(0) cryogel was collapsed into a membrane-like shape after compression (Figure S7d−f).

Chemical cross-linking is believed to play a key role in shape recovery. Chemical cross-linking of chitosan membranes has been shown to increase the strength but reduce the elongation.[28] In our system, interconnected nanochitin pore walls became stiffer with the extent of cross-linking. For nanochitin-based films, a higher tensile strength was achieved with longer fibrils.[16] Similarly, stronger pore walls are expected from the longer fibrils, resulting in stronger nanochitin cryogels. Interestingly, adjacent pore walls were connected with ultralong NCh fibrils (compare Figure 5b and Figure 5c), an effect that likely enhances the mechanical strength of the system.

At constant NCh concentration (0.4 wt %), increased cross-linker loading led to less interconnected and smaller pore walls, resulting in faster and more efficient cross-linking, as previously discussed (Figure 5e−g). However, the NCh(0.4)/Glu(1.0) cryogels were brittle and, under compression, displayed no shape recovery (Figure S7g,h). This indicates that excessive cross-linking has a negative effect. Therefore, uniform film-like pore walls, better-interconnected morphology, and higher stiffness by chemical cross-linking benefit the shape recovery of nanochitin cryogels and hydrogels.

DOI: 10.1021/acsnano.8b07235
ACS Nano 2019, 13, 2927−2935

CONCLUSIONS

A facile and high-yield (85%) method is proposed to produce ultralong chitin nanofibrils that form shape-recoverable hydrogels and cryogels after a freeze-induced chemical cross-linking. The high stiffness, porosity, and excellent compliance of the hydrogels and cryogels, even if prepared from very diluted aqueous suspensions, offer excellent prospects for nanochitins in the synthesis of advanced materials and in applications that benefit from their properties, including tissue engineering, drug delivery, thermal insulation, and air filtration.

METHODS

Materials. Fresh crabs (*Callinectes sapidus*) were acquired in the local market of Helsinki harbor, Finland. The crabs were cooked and the meat was consumed while the residual shells were collected and purified. Glutaraldehyde cross-linker solution (25%) and 100% acetic acid were purchased from Sigma-Aldrich, Germany. Commercial pH 2 buffer solution (density = 1 kg L^{-1}) and pH 11 buffer solution (density = 1 kg L^{-1}) were purchased from VWR Chemicals, Belgium. All chemicals were used without further purification.

Chitin extraction. The purification steps are briefly summarized as follows: the residual biomass was soaked in 1 M HCl for 12 h followed by treatment with 1 M NaOH for 12 h. These two steps were repeated at least three times. The obtained residual solid was decolorized by immersion in 0.5% (w/w) $NaClO_2$, and the pH was adjusted to 5 using acetic acid, followed by heating for at least for 2 h at 70 °C. The purified chitin solid residues were obtained after washing with distilled water. Finally, the obtained flake chitin solids were crushed using a household blender and stored at 4 °C for further use. Notably, the material was always kept in the wet state (never dried).

Nanofibrillation of Chitin. The chitin solids were subjected to deacetylation following a procedure modified from the literature.[16,22] Briefly, purified chitin was treated with 33% (w/w) NaOH solution at 90 °C for 4 h. Then, the partially deacetylated chitin was washed with water and stored at 4 °C until use. Finally, the partially deacetylated chitin was dispersed in water at a concentration of 0.3% (w/v), and acetic acid was added under stirring to adjust the pH to 3.

The obtained suspension was homogenized (IKA T-25 ULTRA-TURRAX digital homogenizer) at 10000 rpm for 5 min followed by passing only one time through the microfluidizer (M-110P, Microfluidics In., Newton, MA, USA) using 400 and 200 μm chambers at a pressure of 1500 bar. After centrifugation at 10000 rpm for 3 min to remove the large particles, the supernatant was collected as the nanochitin suspension.

Nanochitin Hydrogels and Cryogels. Nanochitin suspensions were concentrated by partial water removal at 90 °C or diluted using acetic acid solution (pH 3), reaching mass concentrations of 0.2, 0.4, and 0.6 wt %. The cross-linker was added to the suspension for given glutaraldehyde/nanochitin mass ratios (1:10, 1:2.5, or 1:1). The respective system was then treated with bath sonication USC-TH (VWR, USA) to mix and remove air bubbles. The resulting suspension was sealed in a 15 mL plastic centrifuge tube and frozen overnight in a refrigerator (−20 °C). For hydrogel synthesis, the frozen nanochitin samples were thawed at room temperature for 2 h. After being washed with water, nanochitin hydrogels were obtained. For the preparation of fast freezing samples, after nanochitin and cross-linker were mixed, the NCh(0.2)/Glu(0.4) system was immersed in liquid nitrogen for 3 min (and stored in refrigerator after freezing).

For cryogel synthesis, the frozen samples were lyophilized for 2 days (FreeZone 2.5, LABCONCO, USA). Samples included physically cross-linked (no cross-linker added), chemically cross-linked (cross-linker/nanochitin = 1:1) hydrogels and cryogels, as well as nanochitin suspensions.

Chemical Characterization. FTIR spectra were recorded in the region of 4000−400 cm^{-1} on a Fourier transform infrared spectrometer using Nicolet 380 (Thermo Scientific, USA). For testing, the purified chitin and nanochitin suspensions were dried at 60 °C to eliminate water from the samples.

Dispersion Stability. ζ-Potential measurements were conducted to access the dispersion stability of nanochitin using a Zeta-sizer ZS90 (Malvern Instruments Ltd.) at 25 °C. The concentrations of all samples were the same (0.1%), the pH was adjusted to ∼3, and the dispersion conductivity was measured to be ∼0.74 mS·cm^{-1}.[9]

Morphology. The nanochitin morphology was observed by transmission electron microscopy (FEI Tecnai 12 Bio-Twin, FEI, USA). A drop of nanochitin suspension (0.01%) was deposited on electron microscope grids coated with carbon-reinforced formavar film and allowed to dry, followed by observation at an acceleration voltage of 120 kV. The cross-sectional morphology of cryogels was evaluated by scanning electron microscope using a Sigma VP (ZEISS, Germany) SEM unit operating at an acceleration voltage of 10 kV. Samples were coated with Pt before examination. The nanochitin dispersion was diluted to 0.001% (w/w) with distilled water, placed on a mica plate, and dried at room temperature. The morphologies of the nanochitin were observed using a Dimension Edge atomic force microscope (Bruker, Germany) in tapping mode using a standard silicon cantilever.

The specific surface area and pore characteristics of the NCh cryogels were determined by N_2 adsorption at 77.35 K on a Micromeritics Tristar II 3020 surface area and pore size analyzer (Micromeritics, USA). Approximately 0.05 g of each sample was degassed at 80 °C for 3 h. The specific surface area was determined by the BET method.

Hydrogel Rheology and Water Absorption. Frequency sweeps for nanochitin hydrogels were applied on an MCR 302 unit (Anton Paar Physica, Austria) equipped with parallel plates PP25/P2 (d = 25 mm). The measurements were conducted under a force of 0.1 N at 23 °C.

Water absorption capacity of the nanochitin hydrogels was calculated from eq 1:

$$\text{water absorption capacity} = \frac{W_t - W_o}{W_o} \quad (1)$$

where W_t and W_o are the weight of hydrogels before and after drying at 105 °C.

Shape Recovery. The shape recovery of nanochitin hydrogels was determined from the height of hydrogels in water. Before analysis, nanochitin hydrogels were pressed and water was removed by using filter paper. After compression, the nanochitin hydrogels were immersed in water or buffer solution to determine the extent of shape recovery (eq 2):

$$\text{shape recovery (\%)} = \frac{H_t}{H_o} \times 100\% \quad (2)$$

where H_o is the height of freshly prepared hydrogel before compression, and H_t is the height of the hydrogel after immersion in water or buffer solution, as a function of time.

Physical and Mechanical Properties. The dimensions (length and diameter) and mass of nanochitin cryogels shaped as cylinders were measured using a digital caliper and balance (resolution of 0.01 mm and 0.01 mg, respectively). The density of the cryogel (ρ_a) was calculated simply using eq 3:

$$\text{porosity (\%)} = \left(1 - \frac{\rho_c}{\rho_a}\right) \times 100\% \quad (3)$$

where ρ_c is the density of chitin, 1425 g·cm^{-3}.[29] Cylindrical cryogels (∼13 mm diameter and ∼10 mm height) were used for dynamic mechanical analyses (TA Instruments Q800 DMA, TA, USA) applying strain rate mode (strain rate of 10% strain per min).

DOI: 10.1021/acsnano.8b07235
ACS Nano 2019, 13, 2927−2935

ASSOCIATED CONTENT

Supporting Information

The Supporting Information is available free of charge on the ACS Publications website at DOI: 10.1021/acsnano.8b07235.

FTIR spectra of purified chitin, nanochitin, and chemically cross-linked nanochitin cryogel; photographs of freshly prepared nanochitin suspensions kept at room temperature for 7 days without freezing and in the absence of glutaraldehyde; water absorption capacity of nanochitin hydrogels; photographs of hydrogels after directional freezing; SEM images of hydrogels prepared from nanochitin with different fibril lengths after tip sonication for different times; photographs of shape recovery experiments of NCh hydrogels as a function of nanochitin concentration and pH; photographs of cryogels before and after cycles of compression−relaxation; compressive stress−strain hysteresis measurements for cryogels and respective BET isotherms (PDF)

Shape recovery of NCh(0.1)Glu(0.4) aerogel (AVI)

Shape recovery of NCh(0.2)Glu(0.4) aerogel (AVI)

AUTHOR INFORMATION

Corresponding Authors

*E-mail: fanyimin@njfu.edu.cn.

*E-mail: orlando.rojas@aalto.fi.

ORCID

Long Bai: 0000-0003-3356-9095

Anurodh Tripathi: 0000-0002-3415-0221

Zhiguo Wang: 0000-0003-0201-7220

Yimin Fan: 0000-0003-2764-1310

Orlando J. Rojas: 0000-0003-4036-4020

Notes

The authors declare no competing financial interest.

ACKNOWLEDGMENTS

The authors acknowledge Kivelä Ritva and Dr. Min Huihua for technical support. We are also grateful for access to the facilities of Aalto University Nanomicroscopy Center (Aalto-NMC) and the Advanced Analysis Test Center of Nanjing Forestry University. Funding support was provided by the National Natural Science Foundation of China (No. 31100426) (Y.F.) and the European Research Council (ERC) under the European Union's Horizon 2020 research and innovation program (ERC Advanced Grant Agreement No. 788489, "BioElCell"). We are also grateful to the Foundation for Innovation Training of Graduate Student of Jiangsu Province and the Priority Academic Program Development of Jiangsu Higher Education Institutions (PAPD) for funding the one-year research exchange in Aalto (L.L.).

REFERENCES

(1) Xu, D.; Huang, J.; Zhao, D.; Ding, B.; Zhang, L.; Cai, J. High-Flexibility, High-Toughness Double-Cross-Linked Chitin Hydrogels by Sequential Chemical and Physical Cross-Linkings. *Adv. Mater.* **2016**, *28*, 5844−5849.

(2) Ding, B.; Cai, J.; Huang, J.; Zhang, L.; Chen, Y.; Shi, X.; Du, Y.; Kuga, S. Facile Preparation of Robust and Biocompatible Chitin Aerogels. *J. Mater. Chem.* **2012**, *22*, 5801.

(3) Zhong, C.; Kapetanovic, A.; Deng, Y.; Rolandi, M. A Chitin Nanofiber Ink for Airbrushing, Replica Molding, and Microcontact Printing of Self-Assembled Macro-, Micro-, and Nanostructures. *Adv. Mater.* **2011**, *23*, 4776−4781.

(4) Xie, H.; Zhang, S.; Li, S. Chitin and Chitosan Dissolved in Ionic Liquids as Reversible Sorbents of CO2. *Green Chem.* **2006**, *8*, 630−633.

(5) Hu, X.; Du, Y.; Tang, Y.; Wang, Q.; Feng, T.; Yang, J.; Kennedy, J. F. Solubility and Property of Chitin in NaOH/Urea Aqueous Solution. *Carbohydr. Polym.* **2007**, *70*, 451−458.

(6) Tamura, H.; Nagahama, H.; Tokura, S. Preparation of Chitin Hydrogel under Mild Conditions. *Cellulose* **2006**, *13*, 357−364.

(7) Abe, K.; Ifuku, S.; Kawata, M.; Yano, H. Preparation of Tough Hydrogels Based on β-Chitin Nanofibers *via* NaOH Treatment. *Cellulose* **2014**, *21*, 535−540.

(8) Salaberria, A. M.; Labidi, J.; Fernandes, S. C. M. Different Routes to Turn Chitin into Stunning Nano-Objects. *Eur. Polym. J.* **2015**, *68*, 503−515.

(9) Liu, L.; Wang, R.; Yu, J.; Jiang, J.; Zheng, K.; Hu, L.; Wang, Z.; Fan, Y. Robust Self-Standing Chitin Nanofiber/Nanowhisker Hydrogels with Designed Surface Charges and Ultralow Mass Content *via* Gas Phase Coagulation. *Biomacromolecules* **2016**, *17*, 3773−3781.

(10) Habibi, Y.; Lucia, L. A.; Rojas, O. J. Cellulose Nanocrystals: Chemistry, Self-Assembly, and Applications. *Chem. Rev.* **2010**, *110*, 3479−3500.

(11) Bamba, Y.; Ogawa, Y.; Saito, T.; Berglund, L. A.; Isogai, A. Estimating the Strength of Single Chitin Nanofibrils *via* Sonication-Induced Fragmentation. *Biomacromolecules* **2017**, *18*, 4405−4410.

(12) Ifuku, S. Chitin Nanofibers: Preparations, Modifications, and Applications. In *Handbook of Polymer Nanocomposites. Processing, Performance and Application: Polymer Nanocomposites of Cellulose Nanoparticles*; Pandey, J. K., Takagi, H., Nakagaito, A. N., Kim, H.-J., Eds.; Springer-Verlag: Berlin, 2015; Vol. *C*, pp 165−178.

(13) Fan, Y.; Saito, T.; Isogai, A. Chitin Nanocrystals Prepared by TEMPO-Mediated Oxidation of α-Chitin. *Biomacromolecules* **2008**, *9*, 192−198.

(14) Tsioptsias, C.; Michailof, C.; Stauropoulos, G.; Panayiotou, C. Chitin and Carbon Aerogels from Chitin Alcogels. *Carbohydr. Polym.* **2009**, *76*, 535−540.

(15) Mushi, N. E.; Kochumalayil, J.; Cervin, N. T.; Zhou, Q.; Berglund, L. A. Nanostructurally Controlled Hydrogel Based on Small-Diameter Native Chitin Nanofibers: Preparation, Structure, and Properties. *ChemSusChem* **2016**, *9*, 989−995.

(16) Mushi, N. E.; Butchosa, N.; Salajkova, M.; Zhou, Q.; Berglund, L. A. Nanostructured Membranes Based on Native Chitin Nanofibers Prepared by Mild Process. *Carbohydr. Polym.* **2014**, *112*, 255−263.

(17) Heath, L.; Zhu, L.; Thielemans, W. Chitin Nanowhisker Aerogels. *ChemSusChem* **2013**, *6*, 537−544.

(18) Zhao, D.; Huang, J.; Zhong, Y.; Li, K.; Zhang, L.; Cai, J. High-Strength and High-Toughness Double-Cross-Linked Cellulose Hydrogels: A New Strategy Using Sequential Chemical and Physical Cross-Linking. *Adv. Funct. Mater.* **2016**, *26*, 6279−6287.

(19) Takeshita, S.; Yoda, S. Chitosan Aerogels: Transparent, Flexible Thermal Insulators. *Chem. Mater.* **2015**, *27*, 7569−7572.

(20) Tsutsumi, Y.; Koga, H.; Qi, Z. D.; Saito, T.; Isogai, A. Nanofibrillar Chitin Aerogels as Renewable Base Catalysts. *Biomacromolecules* **2014**, *15*, 4314−4319.

(21) Monteiro, O. A. C.; Airoldi, C. Some Studies of Crosslinking Chitosan-Glutaraldehyde Interaction in a Homogeneous System. *Int. J. Biol. Macromol.* **1999**, *26*, 119−128.

(22) Fan, Y.; Saito, T.; Isogai, A. Individual Chitin Nano-Whiskers Prepared from Partially Deacetylated α-Chitin by Fibril Surface Cationization. *Carbohydr. Polym.* **2010**, *79*, 1046−1051.

(23) Mirzaei, B. E.; Ramazani, S. A. A.; Shafiee, M.; Danaei, M. Studies on Glutaraldehyde Crosslinked Chitosan Hydrogel Properties for Drug Delivery Systems. *Int. J. Polym. Mater.* **2013**, *62*, 605−611.

(24) Jiang, F.; Hsieh, Y.-L. Super Water Absorbing and Shape Memory Nanocellulose Aerogels from TEMPO-Oxidized Cellulose Nanofibrils *via* Cyclic Freezing−thawing. *J. Mater. Chem. A* **2014**, *2*, 350−359.

(25) Lu, Y.; Sun, Q.; She, X.; Xia, Y.; Liu, Y.; Li, J.; Yang, D. Fabrication and Characterisation of α-Chitin Nanofibers and Highly

Transparent Chitin Films by Pulsed Ultrasonication. *Carbohydr. Polym.* **2013**, *98*, 1497−1504.
(26) Fukuzumi, H.; Saito, T.; Isogai, A. Influence of TEMPO-Oxidized Cellulose Nanofibril Length on Film Properties. *Carbohydr. Polym.* **2013**, *93*, 172−177.
(27) Jiang, F.; Hsieh, Y. Lo. Amphiphilic Superabsorbent Cellulose Nanofibril Aerogels. *J. Mater. Chem. A* **2014**, *2*, 6337−6342.
(28) Mi, F. L.; Kuan, C. Y.; Shyu, S. S.; Lee, S. T.; Chang, S. F. Study of Gelation Kinetics and Chain-Relaxation Properties of Glutaraldehyde-Cross-Linked Chitosan Gel and Their Effects on Microspheres Preparation and Drug Release. *Carbohydr. Polym.* **2000**, *41*, 389−396.
(29) Li, J.; Revol, J. F.; Naranjo, E.; Marchessault, R. H. Effect of Electrostatic Interaction on Phase Separation Behaviour of Chitin Crystallite Suspensions. *Int. J. Biol. Macromol.* **1996**, *18*, 177−187.

DOI: 10.1021/acsnano.8b07235
ACS Nano 2019, 13, 2927−2935